

CHAPTER 18 EXPERIMENTAL STUDY ON DYNAMIC BEHAVIOR OF ROCK JOINTS

Mikko P. Ahola^a, Sui-Min Hsiung^a, and Dan D. Kana^b

^aCenter for Nuclear Waste Regulatory Analyses, ^bSouthwest Research Institute, 6220 Culebra Road, San Antonio, Texas, 78238, USA

ABSTRACT

This chapter presents a comprehensive evaluation of the dynamic behavior of rock joints based on both experimental studies in the laboratory on natural and simulated rock joints as well as an actual underground case study. The laboratory single jointed dynamic tests made use of natural rock joints in a welded tuff, and were tested under both harmonic and earthquake loading conditions at various frequencies under displacement control. Experimental results showed that the shearing resistance could be markedly different between the forward and reverse shearing directions depending on the joint roughness, with the shear resistance in the reverse direction being smaller. This is explained to be a direct consequence of the irregular roughness and interlocking nature of the mated joint surfaces. It was also found that the joint dilation that takes place during forward shearing is fully recovered during shear reversal, with a small offset due to gouge buildup within the joint. A laboratory-scale model experiment was also conducted to study the dynamic behavior of a system of interconnected (artificial) joints around a circular opening in scaled down rock mass when subjected to earthquake shear wave motion at the base. Results showed that the primary mode of deformation of the rock mass around the tunnel was due to stick-slip behavior along the joints. This type of stick-slip behavior was confirmed during an actual 3 year underground seismic field experimental program designed to study the effect of relatively low-magnitude, repetitive seismic motion (i.e., mining induced) on the behavior of mined excavations. This stick-slip behavior as evidenced in both the field and laboratory seems to explain quite well the phenomenon of the excavations responding to some seismic events but being unresponsive to others. It is believed that the joint stick-slip behavior forms a basis for the progressive accumulation of joint permanent deformation and, consequently, rock mass fatigue. Since materials are normally weaker under fatigue conditions, it is suggested that similar, or even more, damage to an excavation may be realized through a number of seismic events with relatively smaller magnitudes, as opposed to the damage due to a single seismic event with a strong motion.

CHAPTER 18 EXPERIMENTAL STUDY ON DYNAMIC BEHAVIOR OF ROCK JOINTS

Mikko P. Ahola^a, Sui-Min Hsiung^a, and D.D. Kana^b

^aCenter for Nuclear Waste Regulatory Analyses, ^bSouthwest Research Institute, 6220 Culebra Road, San Antonio, Texas, 78238, USA

18.1 INTRODUCTION

In many cases, the deformation of the rock surrounding an excavation occurs primarily along the natural joints, bedding planes, or blast-induced fractures. The deformation along such interfaces may result from pseudostatic loadings due to excavation of tunnels, as well as thermal loads in the case of underground nuclear waste storage. Deformation along the joints may also be a result of dynamic loadings due to seismic motion from earthquakes. In the case of permanent underground storage of high-level nuclear waste, in which design criteria impose more stringent requirements than ordinary excavations, and long periods of performance are required, the dynamic effects on rock joints need to be considered. This need is especially true in countries such as the United States, where current site investigations for high-level nuclear waste repositories are in seismically active geologic regions. Limited studies on underground excavations have indicated that damage can take place due to fault or joint slip, rock burst, and prolonged or repetitive seismic shaking. Experimental measurements in the field, as well as in laboratory-scale model tests of a jointed rock mass, indicate that successive episodes of dynamic loading on joints result in progressive accumulations of shear displacements (plastic deformation) along the joints (Brown and Hudson, 1974; Hsiung et al., 1992a and 1992b). Failure of excavations can occur when sufficient accumulated joint shear displacements take place. Permanent cumulative displacements, which occur when the rock joint strength is exceeded are often estimated based on material properties obtained under static conditions. As a result, if such properties deteriorate during dynamic loading, analyses of excavation behavior under dynamic loading may be nonconservative.

Several studies have been conducted to understand the dynamic behavior of rock joints. Gillette et al. (1983) conducted dynamic direct shear experiments on artificial rock joint specimens (Loveland sandstone) under both drained and undrained conditions. Tests were carried out at frequencies ranging from 0 to 10 Hz and normal stresses ranging from 69 to 3,448 kPa. They observed that varying frequencies did not significantly alter the response behavior of the individual specimens. However, the behavior of the different specimens was markedly different due to variation in sample geometry. Gillette et al. (1983) also showed that the velocity effects for most rock samples tested were normal stress independent. Although there was some scatter in the experimental data, they did find a general trend indicating increasing shear strength with increasing shear velocity for their tests on Loveland sandstone. This scattering of data was determined to be most likely due to properties of the sample geometry and mating characteristics. Crawford and Curran (1981) conducted tests over a wider range of rock types. Their results indicated that, in general, the shear resistance of harder rocks decreased with increasing velocity greater than a variable critical velocity. The shear resistance of softer rocks increased with

increasing velocity up to a critical velocity. The basic conclusion of these two different studies on dry rock joints is that the rate-dependent strength and shear stress-shear displacement response behavior may have a pronounced influence on rock mass behavior during seismic motion, and it may be important to include such features in dynamic analyses of discontinuous rock masses. Dynamic tests on undrained rock joints by Gillette et al. (1983) showed that the interstitial water pressure in a joint subjected to dynamic shear displacements stabilizes early in the process and does not continue to increase with increasing displacement cycles. They did find that the pressure fluctuated in a manner closely related to joint dilation or contraction. The strength of the joint closely followed the effective stress law even during the highly fluctuating water pressures.

Bakhtar and Barton (1984) conducted large-scale dynamic friction experiments on artificially fractured blocks of sandstone, tuff, granite, hydrostone, and concrete. The fracture surfaces had surface areas of approximately 1 m^2 and were tested under shear velocities in the range of 400 to 4,000 mm/sec. Using modified stress transformation equations along the angle of inclination of the joint as well as joint property characterization methods developed by Barton and Choubey (1977), Bakhtar and Barton were able to predict the measured rock joint strengths to an accuracy of $\pm 15\%$. When they partitioned the tests as pseudostatic or dynamic, the average predicted shear strengths were approximately 5% lower than measured under pseudostatic conditions and 10% lower than measured under dynamic conditions. Thus, their joint behavior model is slightly conservative, and the dynamic strength may be approximately 5% higher than the static strength when shear displacement velocities of approximately 0.001 to 0.1 mm/sec (pseudostatic) are compared with the dynamic velocity range of approximately 400 to 4,000 mm/sec.

Direct shear testing of single-rock joints under dynamic loading was also conducted by Barla et al. (1990). They tested the dynamic behavior of saw-cut surfaces of a dry quartzitic sandstone (Monticello sandstone) up to 100 mm in diameter under a single shear load impulse and constant normal load. The dynamic shear strength was observed to be greater than the corresponding static value and also to increase with increasing shear stress rate. The normal stress appeared to decrease the rate of increase of the dynamic shear strength with respect to the static value. In other words, they found for these single shear load impulses that the larger the normal stress, the smaller the dependence of the dynamic shear strength on the shear stress rate. These results tend to contradict those presented by Gillette et al. (1983), which showed little velocity dependence on the normal load. However, the type of joint surface was quite different in these studies (i.e., saw cut in one case and artificially fractured in the other). The discrepancies are also likely due to the fact that these dynamic tests were conducted using an impulse load which is different from the cyclic joint loading used by Gillette et al. (1983) which assumed the shear velocity built up to the maximum value over a finite time period depending on the input frequency.

Hobbs et al. (1990) also studied the dynamic behavior of rock joints and observed changes in the joint frictional response as a result of perturbation in the sliding velocity. They explained the frictional shear response in terms of cohesion and friction angle evolution laws which were observed to be of a softening character.

To develop a comprehensive database for characterizing the dynamic behavior of rock joints and to aid in the validation of existing rock joint models, extensive laboratory experiments

were conducted at the Center for Nuclear Waste Regulatory Analyses (CNWRA) on single, natural rock joints. The natural rock joint specimens, collected from the Apache Leap tuff site near Superior, Arizona, USA, were tested under two types of dynamic shear loading conditions with various frequencies. These two loading conditions were harmonic and earthquake loads. The dynamic direct shearing was conducted in a displacement-control mode under various normal loads, frequencies, and displacement amplitudes. During the test, the top rock block was sheared with respect to the bottom block. In addition to the experiments on single jointed rocks, a laboratory-scale model experiment was conducted to study the dynamic behavior of a system of interconnected (artificial) joints around a circular opening in a scaled down rock mass when subjected to earthquake shear wave motion at the base. Finally, an actual field experimental program was conducted over a period of about 3 yr to investigate the effect of relatively low-magnitude, repetitive seismic motion on the behavior of mined excavations at the Lucky Friday Mine located in the Coeur d'Alene Mining District in the Idaho panhandle region.

18.2 DYNAMIC BEHAVIOR OF SINGLE NATURAL ROCK JOINTS

Extensive laboratory experiments on the dynamic behavior of single, natural rock joints were recently performed by Hsiung et al. (1994a and 1995a). The natural rock joint specimens for these dynamic tests were collected from the Apache Leap welded tuff near Superior, Arizona, USA, and were tested under two types of dynamic shear-loading conditions with various frequencies. These two loading conditions were harmonic and earthquake loads. This work can be considered as an extension to the dynamic studies discussed earlier, which considered only a single-shear impulse load or at most cyclic harmonic loadings on either saw cut or artificially fractured rock joints. The following sections discuss briefly the dynamic shear testing apparatus as well as recent results of harmonic and earthquake loadings on single rock joints.

18.2.1 Dynamic Shear Testing Apparatus

The servo-controlled direct shear test apparatus used to conduct the dynamic tests (see Kana et al., 1990 and 1992) was described in Chapter 15, which addressed the mechanical-hydraulic behavior of rock joints under direct shearing. The mechanical portion of the apparatus and corresponding instrumentation discussed in Chapter 15 is the same as that used to conduct the dynamic direct shear tests discussed in this chapter. For reference, the basic dynamic direct shear test apparatus and instrumentation channels are shown again in Figure 18.1. The change in the instrumentation plan for the dynamic tests was that accelerometers were mounted to the rock specimen near the joint interface. The horizontal actuator was operated in a displacement-control mode for all the dynamic tests. To conduct the dynamic shear tests under higher normal loads of up to 5 MPa, a horizontal hydraulic actuator of higher capacity than that used for the pseudostatic tests was required.

18.2.2 Harmonic and Earthquake Input

For the harmonic direct shear tests, the prescribed horizontal shear displacement inputs were sine wave drive signals. The total duration for all the harmonic tests was 30 sec, and the sampling rate was 800 points/sec. The high sampling rate was intended to capture high-frequency responses of joints during harmonic tests. Frequency and amplitude of the input displacement sine

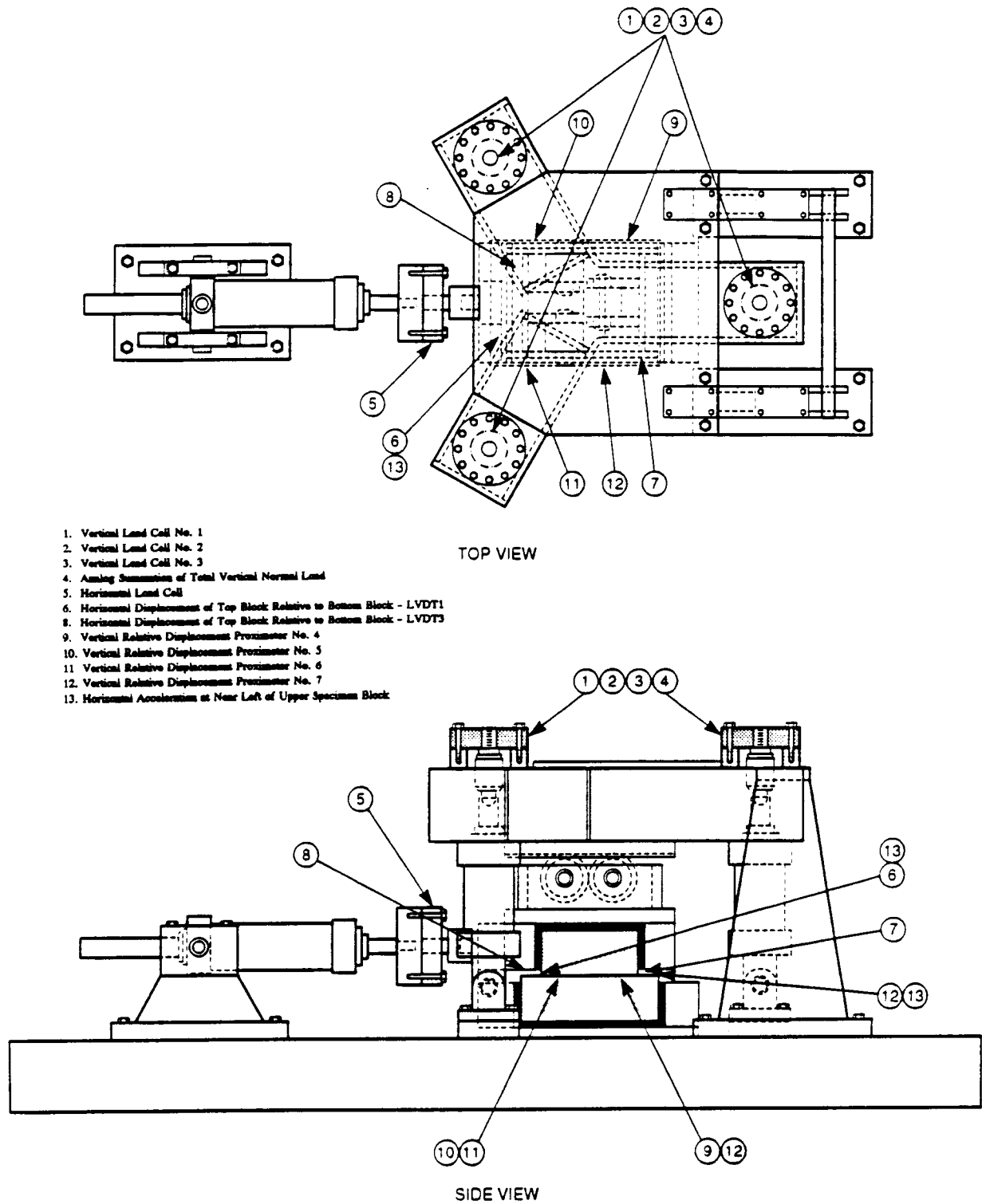


Figure 18.1. Mechanical apparatus for dynamic direct shear testing of rock joints.

wave signal varied for the different tests, with the frequency ranging from 1.4 to 3.5 Hz and amplitude from 6.35 to 25.4 mm. This frequency range was considered to be commensurate with typical earthquake displacement histories. Measurements taken during the harmonic tests included normal and shear loads, joint normal and shear displacements, acceleration responses of the top rock block, and displacement response between the horizontal load cell and the top shear box.

The displacement drive signal used for the joint shear tests under earthquake loads was derived from the acceleration response signal recorded from the Guerrero accelerograph array for the 8.1 Richter scale magnitude earthquake of September 19, 1985, in Mexico. The acceleration response signal measured along the south axis was used to generate a displacement drive signal for the planned joint shear tests subjected to earthquake loads. The initial input displacement drive signal was obtained by double-integration of the windowed acceleration data in the frequency domain (Fourier spectra). Before the double-integration, a bandpass filter was applied to the acceleration Fourier spectra. This filter was defined by low- (0.5 Hz) and high-frequency (15 Hz) values. The high pass filtering was intended to eliminate the possibility of developing extremely large-amplitude, low-frequency offset in the data during integration. Low pass filtering of the points was intended to eliminate aliasing of the data due to its limited sampling rate. Figure 18.2 shows the resulting calculated displacement time history. From spectra analysis, this displacement time history contains a major frequency range from 0 to 2.0 Hz with a dominant frequency at 0.5 Hz. For the various shear tests, two displacement drive signals were used, one with a peak drive signal of 25.4 mm, and 50.8 mm for the other. These two signals were obtained by scaling the displacement signal in Figure 18.2.

18.2.3 Experimental Results of Single Rock Joint Dynamic Behavior

Figure 18.3 shows the measured shear displacement time history and the corresponding shear stress response for a typical test with earthquake load. Only the test results between the 15th and 20th second are presented in the figure for clarity. Results obtained from other earthquake and harmonic tests are similar. There is a phase difference between the shear displacement and shear stress time histories, with the shear displacement lagging. These phenomena were observed for all harmonic and earthquake tests. The source of this phase shift was determined not to be related to the experimental setup. This decision was verified with additional instrumentation. It may be concluded that the phase shift results from shear stress buildup to a level required to initiate joint shear.

As shown in Figure 18.3, the shear stress magnitude increases during forward shearing. The peak shear stress is reached after a certain amount of shear displacement, and the shear stress decreases afterward. However, the shear stress seems to experience a higher frequency component subsequently, which correlates well with stepwise shear displacements observed in the displacement time history. This higher frequency component appears to be associated with rapid stick-slip (i.e., chatter) of the interface and may be enhanced by the presence of natural vibrational modes in the apparatus, as well. The same behavior is also observed during reverse shearing. This chatter behavior is believed to be excited by the waviness of the joint surface as well as by pieces of rock fragments broken from the joint surface. Visual inspection at the conclusion of each test revealed many rock fragments. When the movement of the top rock block

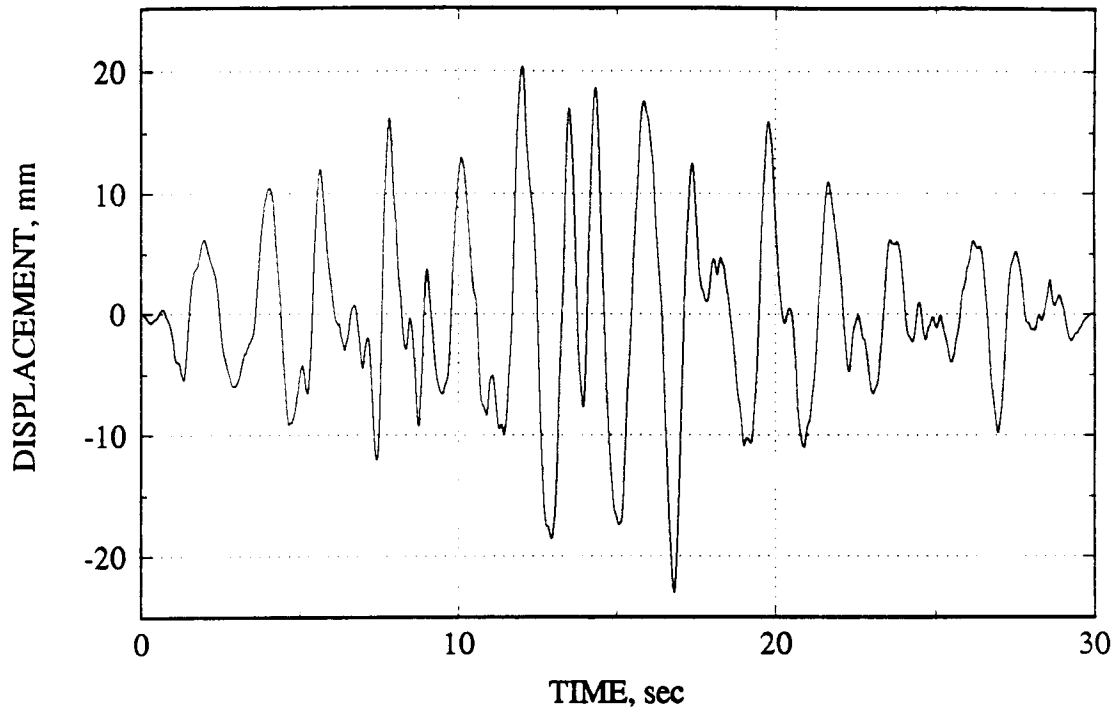


Figure 18.2. Displacement time history generated from the acceleration time history obtained from the 1985 Mexico City earthquake.

is restrained by asperities on the joint surface, it tends to stop until the shear stress is built up sufficiently to overcome this additional resistance by either breaking or riding over the asperity. Depending upon the size and strength of these asperities, the high-frequency responses will vary in amplitude. After the obstacles are overcome, the shear stress drops sharply. There is a period when the shear stress decreases due to cycling. During this period, the shear stress is actually smaller than the shear resistance. Consequently, the top rock block stops until reverse shearing starts when the negative shear stress begins to increase. This behavior is evident by the flattening of the relative shear displacement near its peak values.

Unlike the pseudostatic direct shear tests, the normal stress for the dynamic tests could not be maintained as a constant during the course of the tests as planned. This failure was due to the inability of the servo-controlled valve for the vertical actuators to adjust quickly to the sudden changes in the normal stress in response to changes in asperities during shearing. For the harmonic tests conducted under an applied normal stress of 1.0 MPa, the normal stress fluctuated as much as 0.3 MPa. It is reasonable to conclude that, as the normal stress increases, its normalized variation (presented as percentage of change) decreases, and so does the potential impact of normal stress variation for the dynamic tests. Also, the vibration mode of the normal stress is not exactly synchronized with that of the normal displacement, and the variation of the normal displacement at high frequency is quite small. Therefore, it may be concluded that the effect of normal stress variation is likely to be small. The extent of the effect of normal stress variation on the shear response at the low normal stress level is difficult to judge. However, given the transient nature of the variation, its impact should also be small.

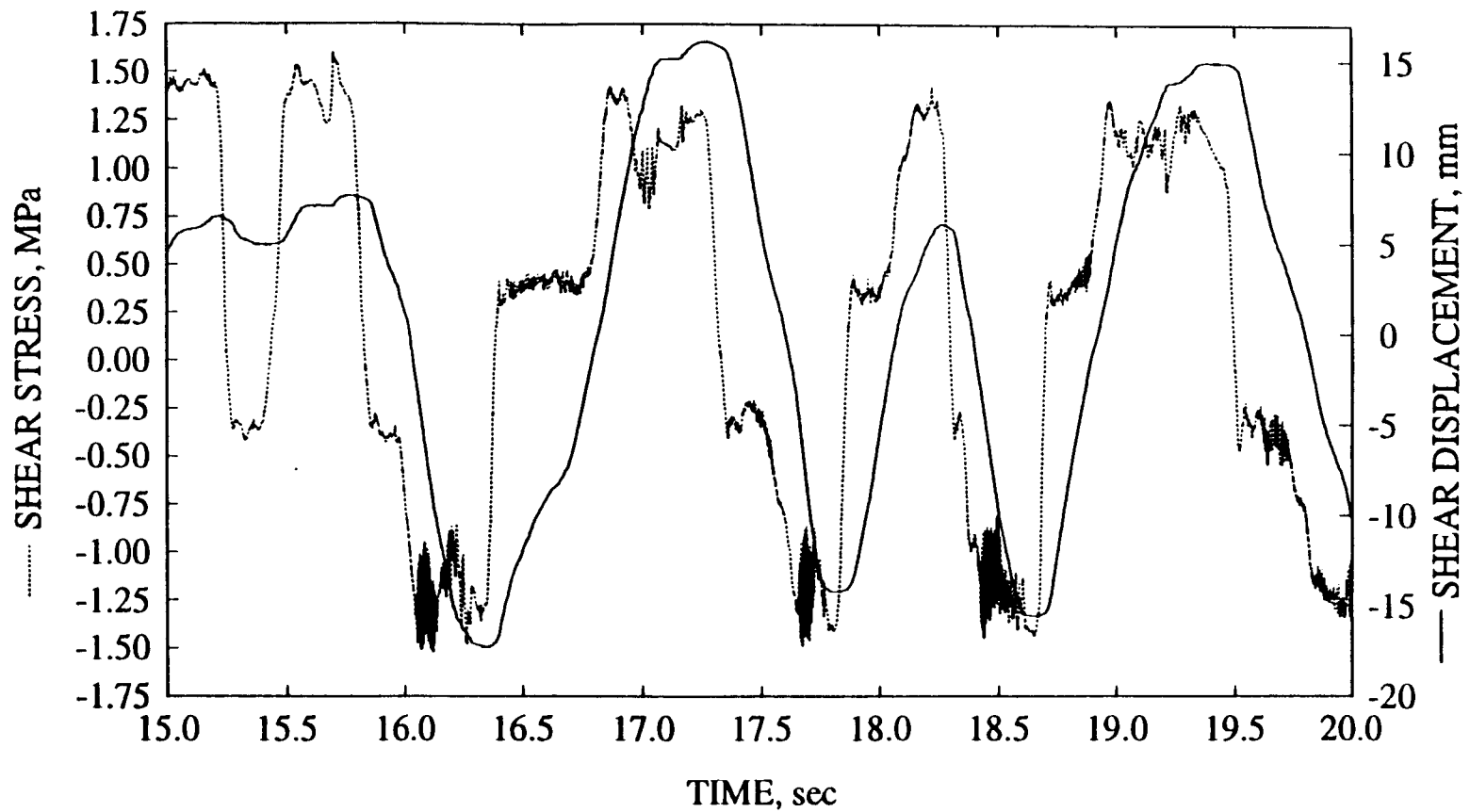


Figure 18.3. Shear stress and shear displacement history between the 15th and 20th seconds of Test No. 25 using the earthquake signal with maximum nominal input displacement amplitude of 25.4 mm under 1-MPa normal stress.

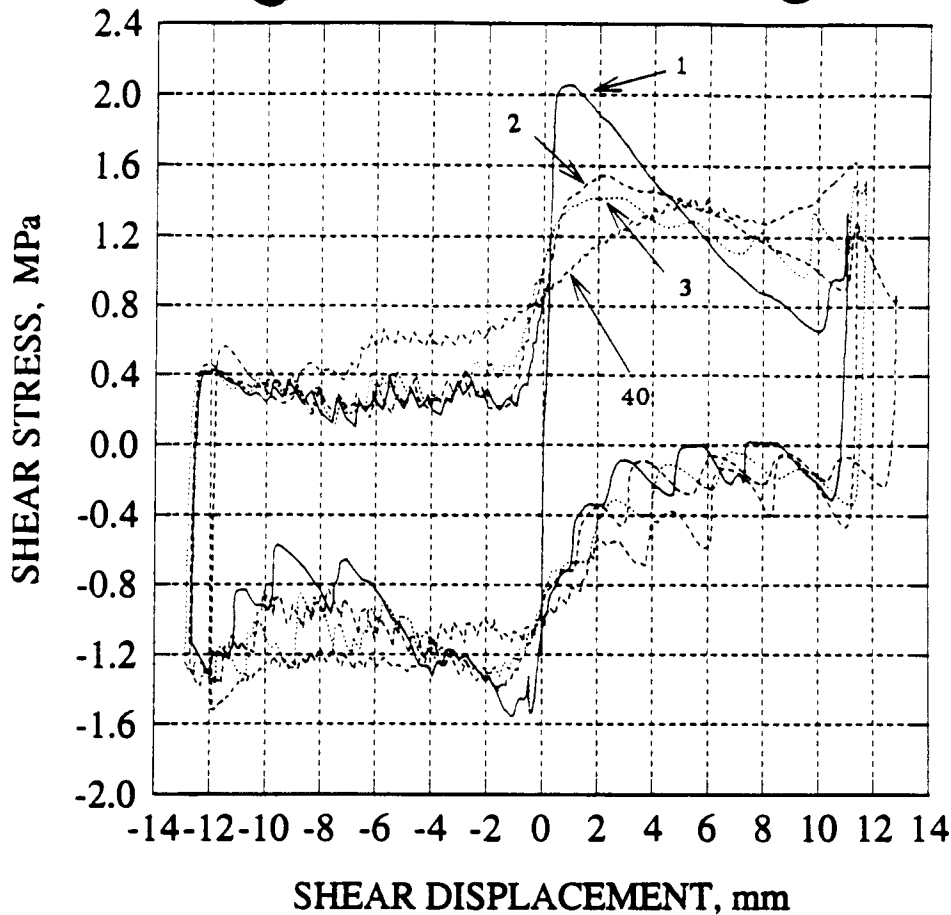


Figure 18.4. Shear stress versus shear displacement curve for the first phase of Test No. 14 under a harmonic load with 1.4-Hz input frequency and 12.7-mm input displacement amplitude (first three cycles and 40th cycle).

Figure 18.4 shows the characteristic hysteresis from Test Number 14 of the joint shear stress versus joint shear displacement from dynamic shear testing using a harmonic input motion with a 1.4-Hz input frequency and an amplitude of 12.7 mm. The test was conducted under a constant normal stress of 1.0 MPa for a duration of 30 sec. Only the response from the first three cycles as well as the 40th cycle are plotted. For these tests, the experiment started with the shearing of the top rock block from its original centered position (represented as 0 shear displacement in the figure) toward one end of the bottom rock block until a predetermined maximum value of shear displacement (positive to the right) was reached. The corresponding shear stress versus shear displacement characteristic curve with this portion of shearing is shown in the first quadrant of Figure 18.4 (from 0 to +12 mm displacement). After the maximum shear displacement in the first quadrant was reached, the top rock block began to move back toward (from +12 to 0 mm displacement) and eventually past its original position (from 0 to -12 mm displacement). The corresponding shear stress versus shear displacement characteristic curves are presented in the fourth and third quadrants of the figures, respectively. After the maximum shear displacement in the third quadrant was reached, the top rock block moved again back to its

original position (from -12 to 0 mm displacement) to complete a cycle of shear motion. The associated shear stress versus shear displacement characteristic curve is presented in the second quadrant of the figure. This process was repeated for a number of cycles. Again, these tests were set up to have the top block mated in the middle of the bottom block to allow the top block a maximum allowable travel of about 50.8 mm on either side of the original position along the direction of shearing. As shown in the figure, the shear stress is assigned to be positive when the shearing is along one direction and becomes negative when the shearing follows the opposite direction. Consequently, the sign for the shear stress denotes the direction of the shear instead of the magnitude of the shear stress. Similarly, Figure 18.5 shows the characteristic hysteresis of the joint shear stress versus joint shear displacement for the first phase of Test Number 30 under earthquake loading.

As was observed in pseudostatic tests, a peak joint shear stress (peak joint shear resistance) was observed for the first cycle for both the harmonic and earthquake shear tests provided the jointed specimens used for the tests had never been shear tested previously or showed signs of past shearing before sample collection. The phenomena of wear of the joint are also clear, shown in Figures 18.4 and 18.5, as the shear stress (joint shear resistance) decreases with the number of cycles. Throughout this chapter, the term forward shearing is used to indicate that the top rock block moves away from its original position, while reverse shearing denotes that the top rock block moves toward its original position.

One distinct feature of the shear stress versus shear displacement characteristics in Figures 18.4 and 18.5 is the smaller shear resistance upon reverse shearing as compared to that of forward shearing (the first quadrant versus the fourth quadrant, the third quadrant versus the second quadrant). This same behavior is similarly observed on pseudostatic tests on the Apache Leap natural tuff joints and reported by other researchers (Jing et al., 1992; Wibowo et al., 1992; Huang et al., 1993) for rock replicas under pseudostatic loads. Both the forward and reverse shearing are likely important phenomena for a rock joint when it is subjected to earthquake loads, whereas only forward shearing is of concern under static loading. The low shear resistance associated with the reverse shearing process may play a key role in determining the stability of an underground opening if the condition is unfavorable. Therefore, a better understanding of the cause of this observation is important to the design of a stable underground excavation.

Jing et al. (1992) implied that, on a larger scale, a rock joint surface contains dominant wavelengths called "primary asperities." There also exist, on the joint surface, "higher order asperities" that have much smaller sizes as compared to the primary asperities [Figure 18.6(a)]. Profiles taken from the Apache Leap tuff joints confirm the existence of the primary and higher order asperities. Three factors have been suggested (Jing et al., 1992) to affect joint shear behavior: higher order asperities, amplitude to wavelength ratio of the joint surface curvature, and basic friction angle of the rock. The higher order asperities and the basic friction angle of rock provide the fundamental joint resistance to shear, while the amplitude to wavelength ratio determines the magnitude of the tangential component of the normal vertical stress along the curved surface. Depending upon the direction of shear, this tangential component could either increase or decrease joint shear resistance. As shown in Figure 18.6, when the top rock block is moving upslope, the "local" direction of shear is opposite to the direction of the tangential component. Consequently, more shear is needed to overcome this tangential component. When

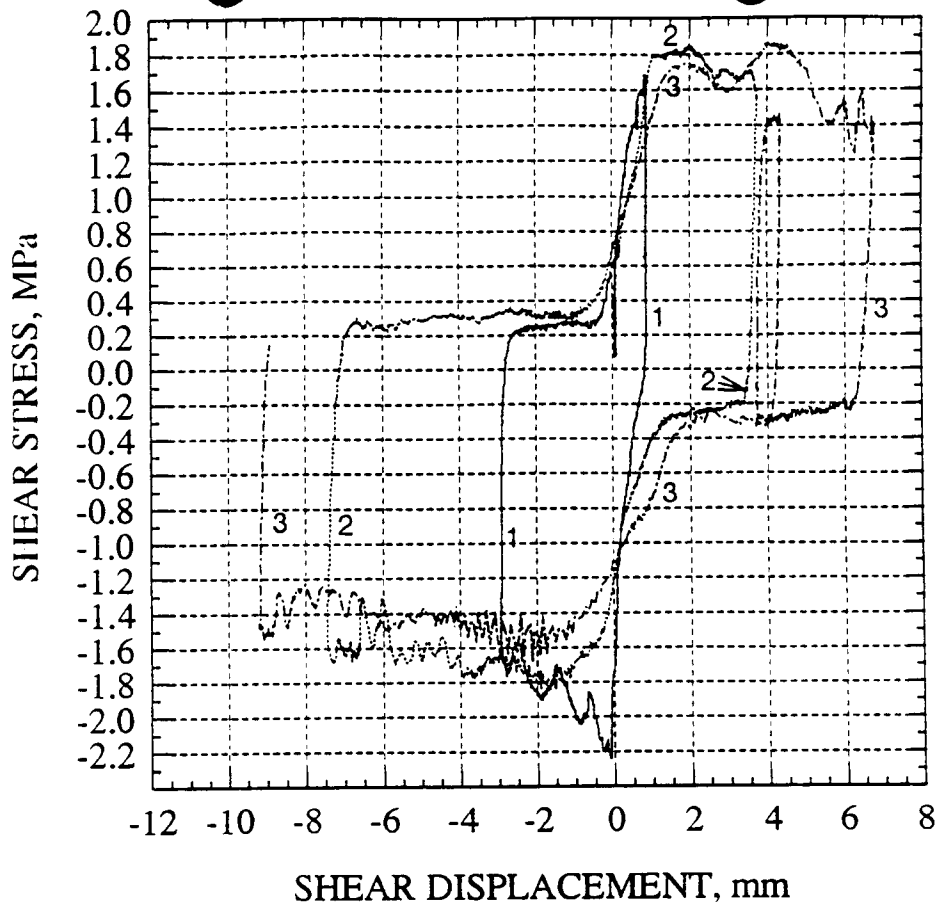


Figure 18.5. Shear stress versus shear displacement curve for the first phase of Test No. 25 under an earthquake load with a maximum input displacement amplitude of 25.4 mm.

the top block moves downslope, the local direction of shear is the same as that of the tangential component of the normal stress. As a result, relatively smaller shear stress is required to overcome the mobilized friction. This concept explains quite well the phenomenon observed in Figure 18.4. Another important factor not included in the hypothesis proposed by Jing et al. (1992) that may also contribute to the difference in shear resistance between forward and reverse shearing is the normal component of the system shear stress applied to the curved surface. When the top block is climbing upward along a primary asperity, a portion of the applied shear stress (horizontal stress) actually becomes localized normal stress, τ_{sn} , as shown in Figure 18.6(b), which tends to resist shear. As a result, the actual localized shear stress becomes smaller than the system shear stress, τ_s . Consequently, more system shear stress is required to overcome this additional normal stress in order to mobilize the joint. On the other hand, if the top rock block is moving downslope, this normal component of the system shear stress tends to offset the applied local normal stress [Figure 18.6(c)]. As a result, a smaller shear stress is required to mobilize the joint.

In many cases, the shear stress continued to increase and decrease about the mean value during the course of harmonic or earthquake loading. These fluctuations in shear stress are a result

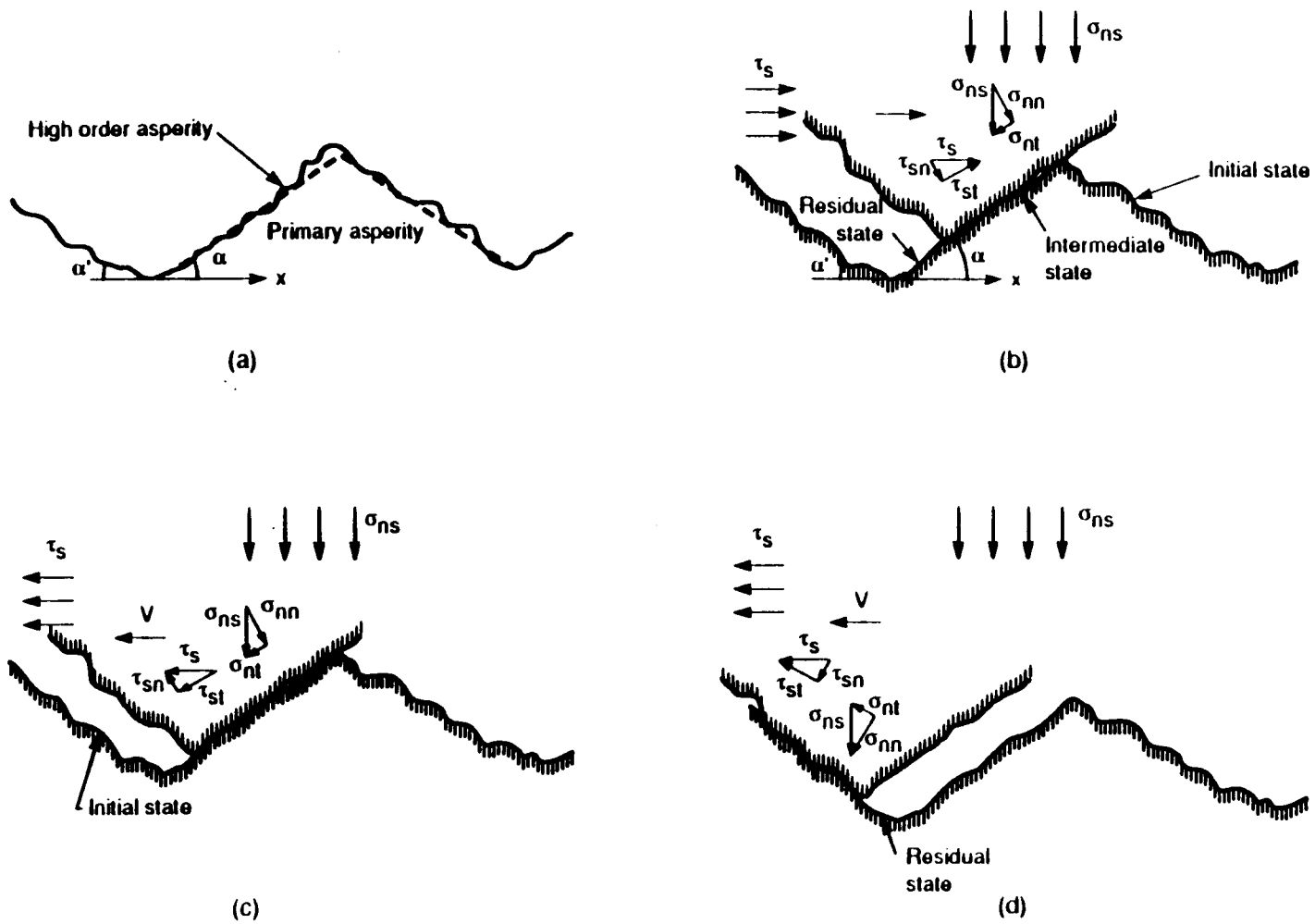


Figure 18.6. Hypothesis of joint shear behavior during forward and reverse stages.

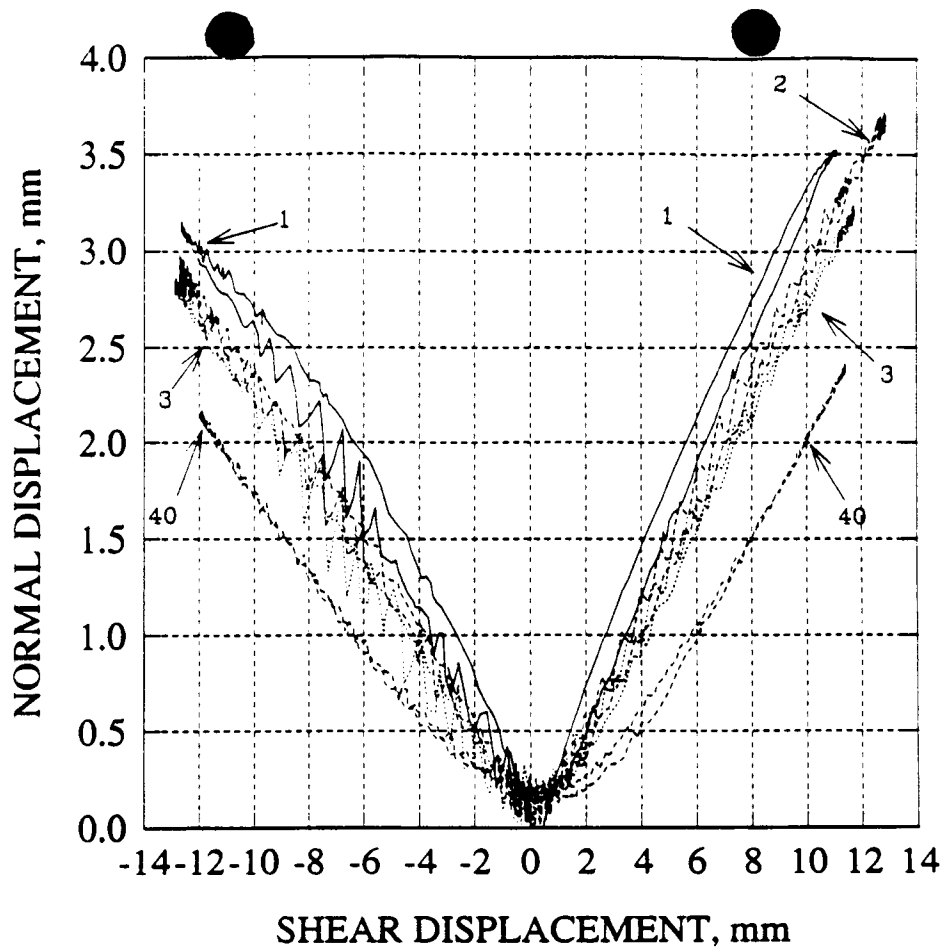


Figure 18.7. Joint normal displacement (dilation) versus shear displacement for the first phase of Test No. 14 under a harmonic load with 1.4-Hz input frequency and 12.7-mm input displacement amplitude (first three cycles and 40th cycle).

of asperities or rock fragments encountered during the shearing process, commonly referred to as stick-slip behavior. Based on the experimental results, these fluctuations in shear stress or chatter become increasingly pronounced with increase in input frequency, although the applied normal stress was 1 MPa. It is also interesting to note that, in some cases of the dynamic tests, the chatter behavior continued even after a number of cycles of shearing.

Since natural rock joints were used for the direct shear tests under harmonic and earthquake loading conditions, a different joint specimen was needed for each test. The fact that each jointed specimen had its own characteristic roughness made it difficult to evaluate directly the dynamic effect on the joint shear resistance as was done in studies by other researchers using saw-cut joints or replicas. However, based on the present dynamic studies, it was established that the difference between joint shear resistance during reverse shearing and peak shear resistance will be larger for joints with rougher surfaces. In other words, for such joints the shear resistance during reverse shearing will be much smaller compared to the shear resistance during forward shearing.

Figure 18.7 shows the joint normal displacement versus shear displacement characteristic curve corresponding to Figure 18.4 for Test No. 14 under harmonic load. Likewise, Figure 18.8

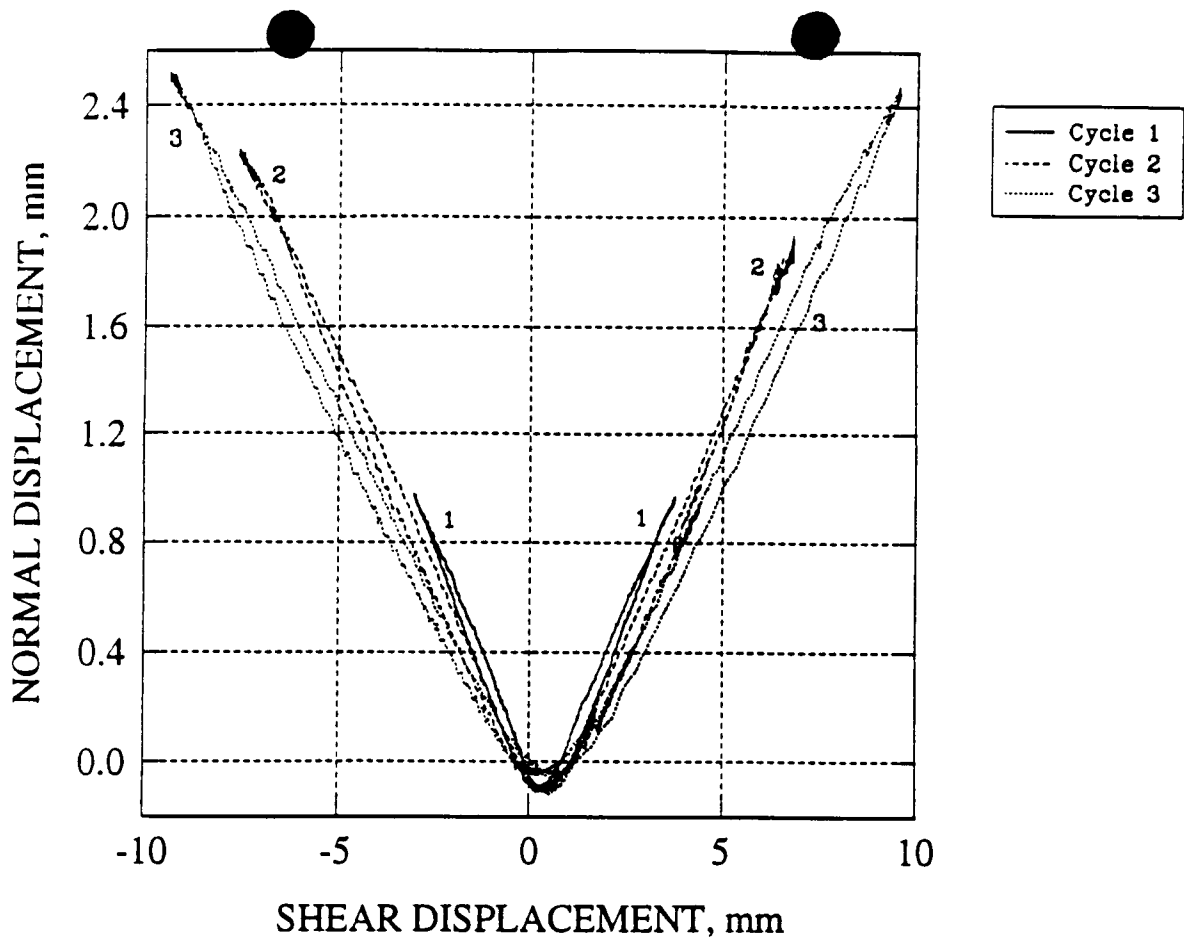


Figure 18.8. Joint normal displacement (dilation) versus shear displacement of the first phase of Test No. 25 under an earthquake load with a maximum input displacement amplitude of 25.4 mm.

shows a similar plot obtained under earthquake loading, corresponding to Figure 18.5. Again, from Figures 18.7 and 18.8, the effect of the continuing wear of the joint surfaces is evident. The maximum joint normal displacement continues to decrease through the cycles of shearing. It is interesting to note that joint dilation (positive normal displacement) tends to decrease constantly during reverse shearing and may retain a small amount of dilation as the top rock block returns to its original position. This phenomenon can be explained quite well using the conceptual model shown in Figure 18.6. Dilation reduces when the top rock block goes downslope, which is always the case during reverse shearing if the top and bottom rock blocks are closely matched before the test. However, for the harmonic tests, small-scale stick-slip oscillations were observed to continue for many cycles. This observation gives an indication of the potential impact of the input frequencies on joint dilation, which may be related to the existence of small-size rock fragments created in the process of shearing. The hysteresis between the normal displacements during forward and reverse shearing of the first cycle for the harmonic and earthquake tests was determined to be smaller than that observed for the pseudostatic tests.

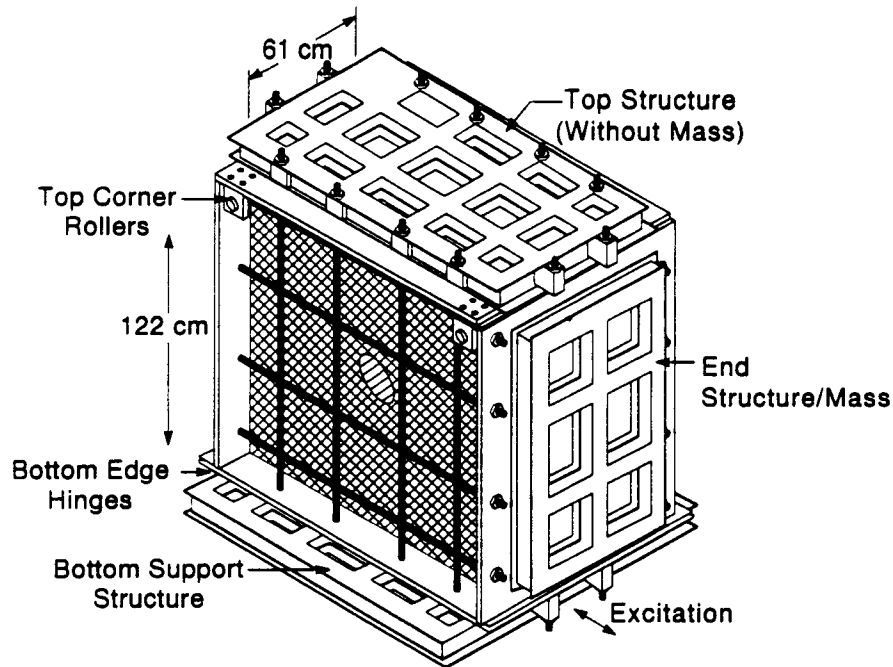


Figure 18.9. Physical design of scale model rock mass with a circular opening.

18.3 DYNAMIC BEHAVIOR OF MULTIPLE ROCK JOINTS (LABORATORY-SCALE MODEL EXPERIMENT)

18.3.1 Description of Scale Model Experiment

As a follow-on to the laboratory dynamic studies on single, naturally jointed, welded tuff fractures, a laboratory-scale model experiment was developed and tested to determine the seismic response near a circular opening in a jointed rock mass (Hsiung, et al., 1995b; Kana et al., 1995). The 1/15-scale model consisted of an aggregate of simulated rock material blocks that were used to study the earthquake response of a larger segment of the proposed rock mass (welded tuff). A detailed discussion of the derivation of the scaling parameters for the scale model material, dimensions, and loading conditions is given by Hsiung et al. (1995b) and Kana et al. (1995). Results of numerical simulation of the experiment using the distinct element approach is given by Hsiung et al. (1994b).

The final physical design and associated values for various parameters are given in Figure 18.9. The model consisted of an aggregate of many rock simulant ingots, each 61 cm long, with the interfaces oriented at a 45 degree angle to the horizontal. The ingot cross-sections varied from 5×5-cm square for basic ingots, to half-section ingots at the boundaries, to curved-section ingots around the center circular opening. This opening was 15.2 cm in diameter. The four boundaries of the stack were interfaced with 6.4-mm thick rubber, which is bonded to the rock on the inside and lubricated with silicone at the interface with the confining box boundaries. These boundaries were a very stiff construction of welded aluminum plates and 10.2-cm I-beam frames. The proper pressure, σ_n , was maintained on the system by eight vertical cables and eight horizontal cables.

The two end structures were hinged to the bottom support structure at the baseplate and were held against top rollers at each upper corner. Therefore, the end structures can pivot laterally, while the top structure can pivot and float up and down as necessary to follow the confined rock motion.

18.3.2 Development of the Rock Simulant

It was recognized that exact modeling of welded tuff behavior was probably neither possible nor was actually necessary for a successful verification of analytical models. Therefore, the technical approach adopted for development of a suitable rock simulant consisted of following the similitude guidelines as much as practical, but allowing deviations as long as they could be quantified. Initial development of the rock simulant was based on repeated trials of various constituent mixtures and testing of material properties of cylindrical specimens cast from these mixtures. The specimens were cast as 5.0-cm (2-in.) diameter by 10.0-cm (4 in.) long specimens that were instrumented with strain gages and tested in uniaxial compression. Table 18.1 lists the ingredients that were ultimately found to provide a material having the appropriate properties.

Table 18.1. Properties of rock simulant specimen

Material Constituents (Percent by Weight)	
Type I Portland Cement	25.2
Barite	45.9
Water	25.2
Bentonite	3.4
DARACEM-100 (Plasticizer)	0.3
Vinsol Resin (Air Entrainment)	8.6×10^{-3}
Ivory Liquid Soap	4.6×10^{-2}
Uniaxial Compressive Strength 10.35–13.79 MPa (1,500–2,000 lb/in. ²)	
Material Density 1,682 kg/m ³ (105 lb/ft ³)	
Roughness Data	
Average Peak:	±0.2 mm (0.008 in.)
Average Wave Length:	6.4 mm (0.25 in.)

Having developed the above described material, it now became appropriate to develop a scale model rough surface. The intent was to cast specimens of the same size as originally used for the single jointed welded tuff blocks and to perform combined normal and shear tests in the same apparatus to obtain data analogous to Figure 18.4 or 18.5. However, it was recognized that scale model conditions also must be considered for these tests. A material was found that produced a random roughness with the average peaks approximately 1/15 geometric scale to those observed for typical welded tuff specimens. However, it was recognized that with each of the two surfaces being independently random, no significant interlocking of surfaces would occur, as was typical for naturally-welded tuff joints. Therefore, the effects of these differences would need to be quantified by shear tests. A series of rock simulant specimens was subjected to

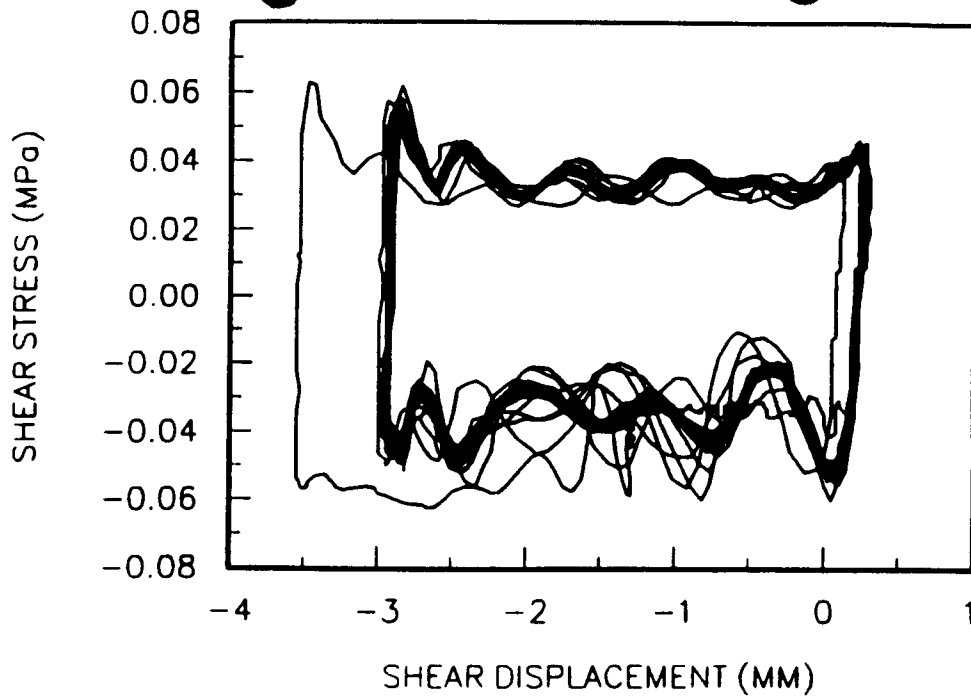


Figure 18.10. Hysteresis for rock simulant under 0.065 MPa normal stress and 5.4 Hz sinusoidal shear.

both pseudostatic and dynamic shear tests. Figure 18.10 shows the results for scaled harmonic tests for a typical rock simulant specimen. By comparing Figure 18.10 with 18.4, it is obvious that, indeed, no offset in hysteresis occurs for the rock simulant. Nevertheless, corresponding friction properties could still be approximated.

18.3.3 Instrumentation and Data Acquisition

It was recognized that rock interface relative normal and shear displacements and overall rock mass motions were of interest and that the transducers used for such measurements should offer negligible resistance to rock interface motion. Therefore, several types of transducers were selected for measurement of these responses. These transducers included accelerometers, strain gages, specially designed cantilever beam shear displacement measurement devices, Bentley proximeters, and linear variable differential transducers. A photograph of some of the instrumentation on and near the tunnel opening is shown in Figure 18.11. It was also recognized that relatively large displacements might be expected for the blocks around the opening due to repetitive shaking. The transducers mentioned earlier were not expected to function under large displacements. Consequently, one video camera was mounted at each side of the scale model apparatus along the axis of the tunnel to capture large displacements.

A block diagram of the 50-channel instrumentation system is shown in Figure 18.12. Data rates were dictated by the capacity of the 486 (66-MHz) digital computer with a 1-gigabyte hard drive, and its associated data acquisition cards. The total duration for each test was 10 seconds. It was determined that 2,800 samples/sec was the fastest data rate feasible for each of 50 data

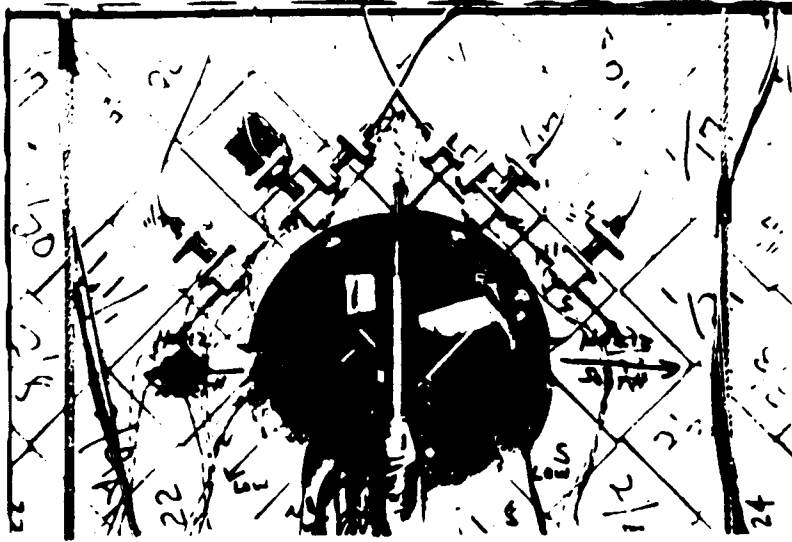


Figure 18.11. Instrumentation on near side of tunnel opening.

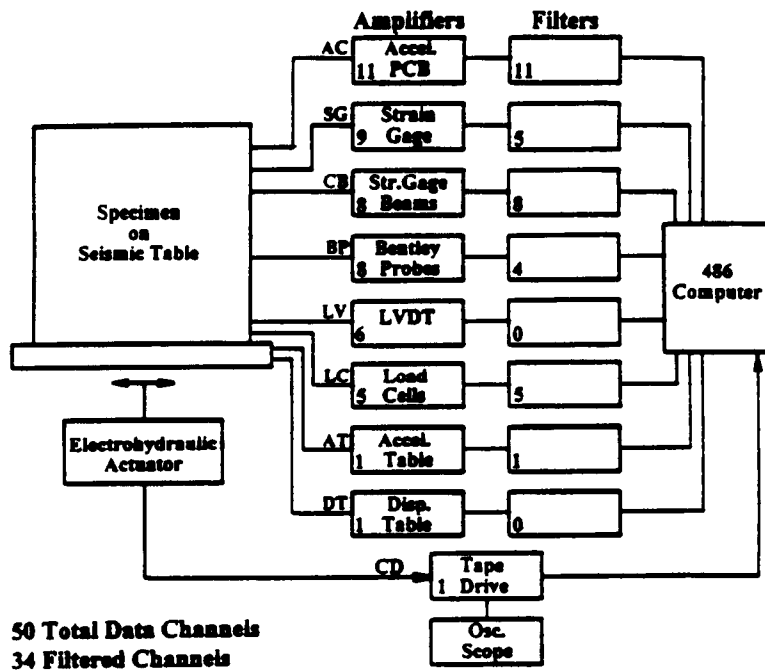


Figure 18.12. Block diagram of data acquisition system.

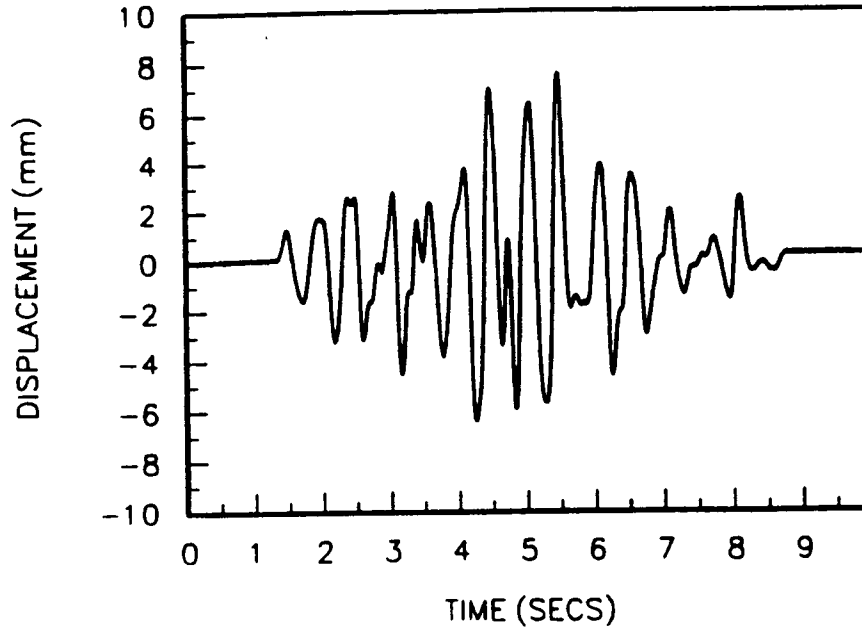


Figure 18.13. Horizontal table displacement for scale model earthquake data set 14: 1.0-cm displacement amplitude.

channels sampled sequentially. Hence, for each run a total of 1.4 million samples of data were acquired.

18.3.4 Test Procedures and Experimental Results

The test runs were started at a very low peak excitation displacement level, and this amplitude was incrementally increased as the runs progressed. Both videotape and digital data were acquired for each run. At the end of each run, all data were converted to engineering units, and a preliminary review of the data was performed visually on the monitor. In some infrequent cases, transducer or other component malfunction occurred, and adjustments were performed prior to the next run. Furthermore, some shifting of filter channels and/or transducer locations was performed as response information was acquired.

The horizontal excitation displacement applied to the seismic shaking table (i.e., base of the scale model rock mass) for the intermediate level run is shown in Figure 18.13. This waveform was again derived from the accelerogram measured at the Guerrero array for the September 1985, Mexico City earthquake. However, unlike the time history used in the single rock joint dynamic tests, the displacement time history waveform in Figure 18.13 represents a 1/15-scale displacement history (i.e., both the time duration and peak displacement amplitude were scaled down). Corresponding to this excitation, permanent shifts in rock ingot positions are evident in the cantilever beam response of Figure 18.14 and the Bentley proximeter response of Figure 18.15. Based on these data, the near side upper right ingot at the opening has shifted

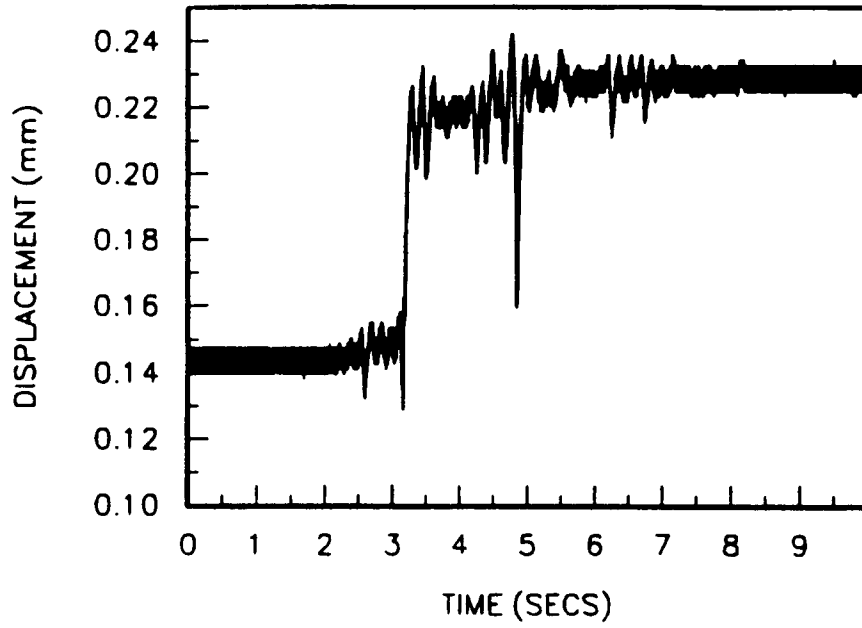


Figure 18.14. Near side tunnel block displacement: CB 4 data set 14, 1.0-cm displacement amplitude.

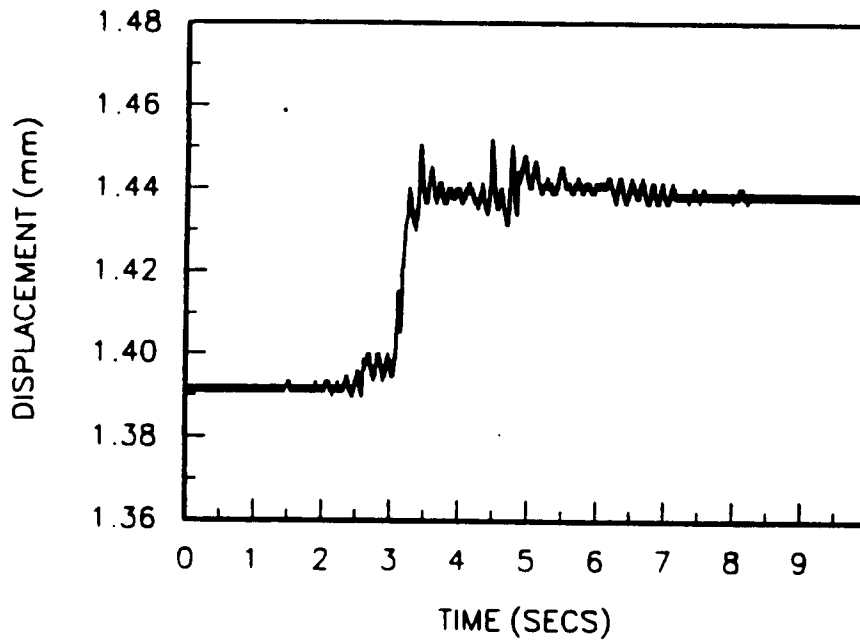


Figure 18.15. Near side left tunnel wall relative displacement; BP 2 data set 14, 1.0-cm displacement amplitude.

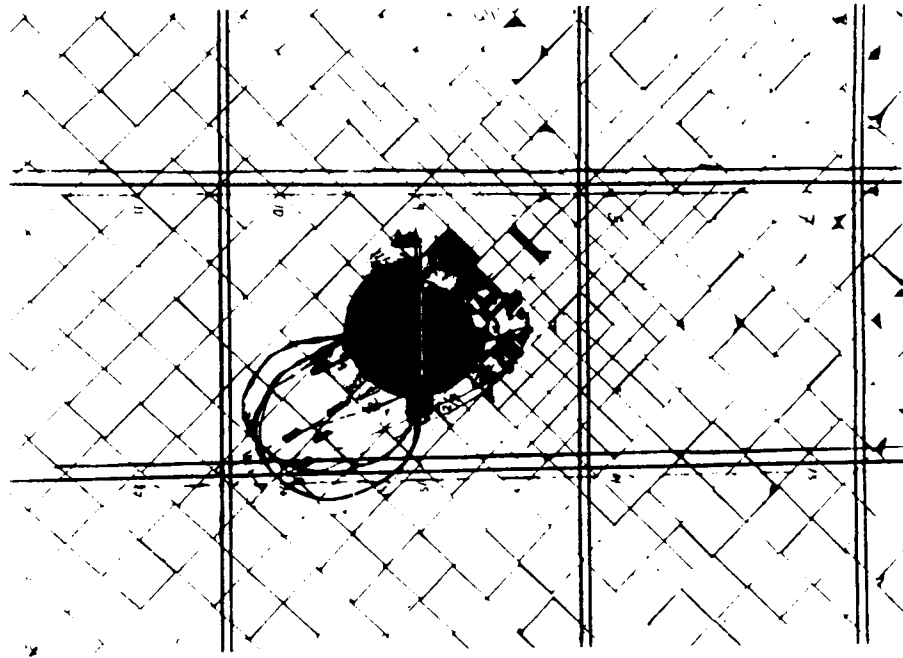


Figure 18.16. Accumulated permanent shift of rock ingots on far side of opening at end of test series.

downward relative to its adjacent ingots. Further analysis of data showed that both upper ingots, as well as those immediately below them, migrated downward radially into the opening, as would be expected under the influence of gravity. This behavior continued for each test run. Figure 18.16 shows the condition on the far side opening face after the test series was completed. It is obvious that very significant joint displacements near the opening have occurred. It was noted that the displacements at the near face were not so pronounced. In fact, a fracture of the one top ingot had occurred near the center along its length, so that the marked differences could accumulate. This behavior probably resulted from nonuniformity in the ingots or loading conditions.

18.4 DYNAMIC BEHAVIOR OF AN UNDERGROUND TUNNEL IN A FRACTURED ROCK MASS (CASE STUDY)

A case study was also conducted to investigate, through field instrumentation, the performance of an underground excavation subjected to repetitive episodes of mining-induced seismic activity. The study was conducted at the Lucky Friday Mine, Mullan, Idaho (Hsiung et al., 1992a and 1992b). The primary purpose was to determine if the progressive accumulation of joint deformation resulting from episodes of dynamic loading has any potentially adverse effect on the performance of underground excavations.

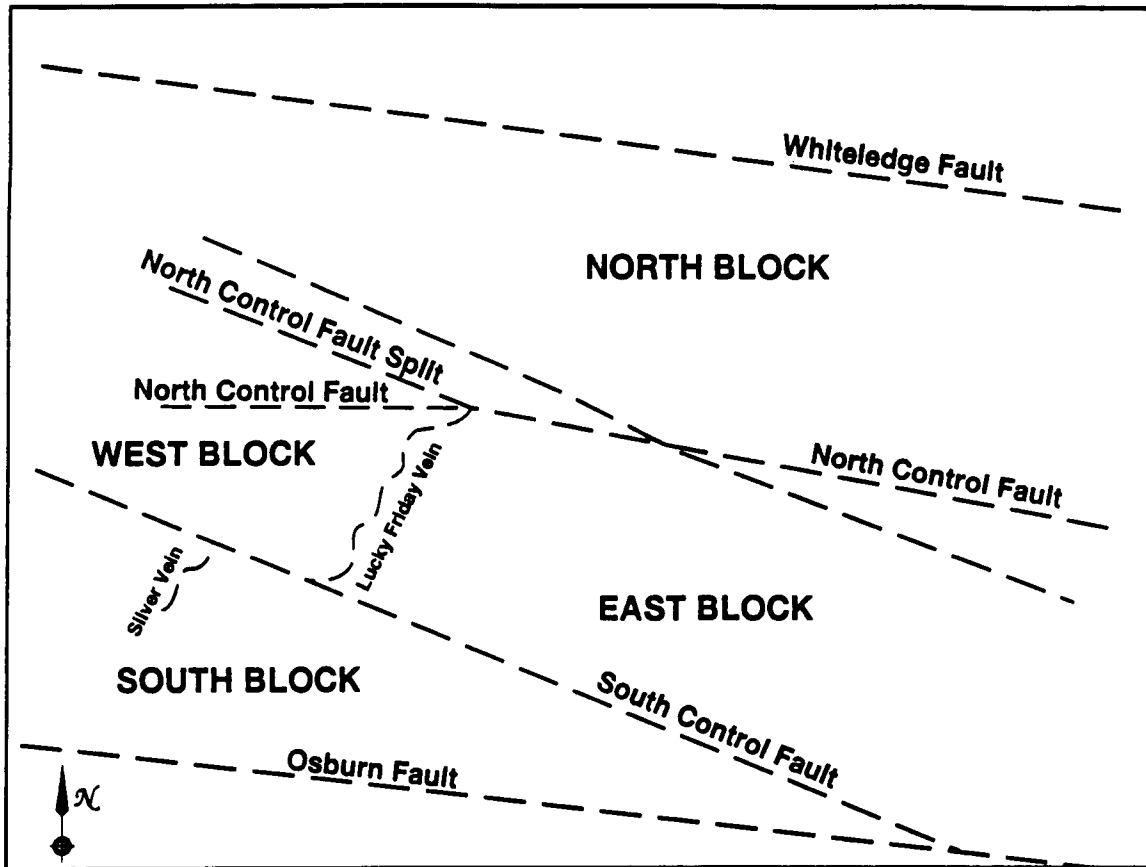


Figure 18.17. Plan view of the Lucky Friday orebody showing fault structures.

18.4.1 Site Description and Instrumentation Layout

The Lucky Friday Mine is located in the Coeur d'Alene Mining District in the Idaho panhandle region. The mining depth is approximately 1,615 m below ground surface. The ore-bearing stratum (called the Lucky Friday vein) generally strike north-east and are nearly vertical with about 457 m of mineable strike length. This vein is bound on its north and south extent by faults and is cut by several major faults (Figure 18.17). The surrounding hanging wall and footwall rock is composed of interbedded units of vitreous quartzite, sericitic quartzite, and greenish siltite-argillite. The bedding planes are sometimes continuous with roughly planar surfaces, which often show evidence of past shearing. The beds dip, in general, south-east with an angle of approximately 70° from the horizontal and strike conformably with the vein. *In situ* stress measurements indicate that the maximum horizontal stress is about 1.35 times the minimum horizontal stress and vertical stress (Board and Beus, 1989). The maximum horizontal stress in the vicinity of the Lucky Friday Mine is oriented N45°W and perpendicular to the striking direction of the vein.

The mine uses the underhand cut-and-fill mining method. The general advance of the mining is downward. Four stopes are used on each level, which advance downward in a series of

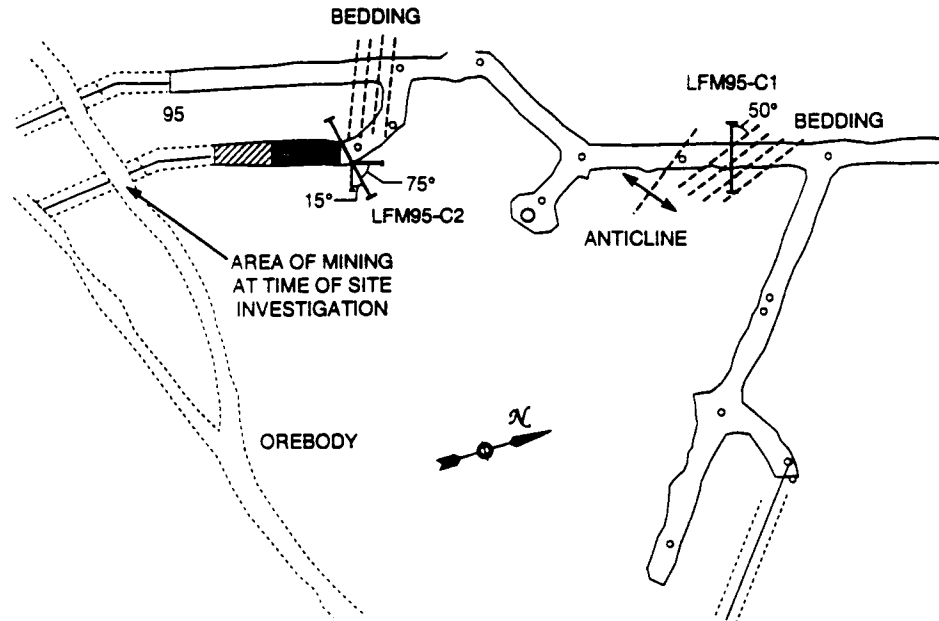
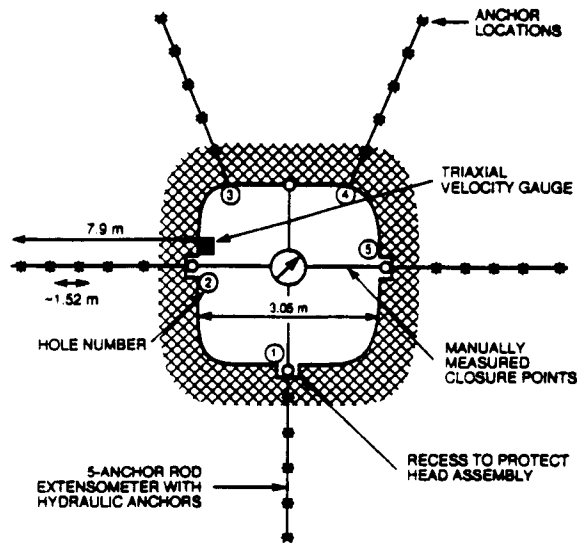


Figure 18.18. Locations of instrumentation at the 5210 level of Lucky Friday Mine.

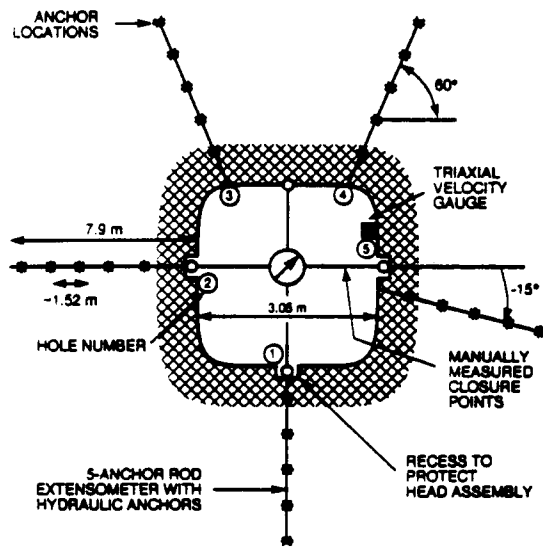
3.05 m high cuts. The haulage development for each stope is a spiralling ramp in the footwall. Most of the seismic events in the mine occurred in the footwall where bedding planes dip toward the orebody.

Two sites near the bottom of the ramp systems under development were selected for instrumentation to monitor rock mass responses around underground excavation under repeated seismic events. Since these two sites were below the stope, they were relatively undisturbed by stoping in the early stages of monitoring. One site (LFM95-C1) was about 1,591 m, and the other (LFM95-C2) about 1,598 m, below ground level. Figure 18.18 shows a portion of the ramp system where the two instrumentation sites were located. The LFM95-C2 site was about 30.5 m from the orebody and the LFM95-C1 site was about 76.2 m away. The bedding planes intersect the instrumentation cross section of the LFM95-C1 site at an approximately 50° angle and at a 15° angle for the LFM95-C2 site. Both sites were supported by 1.8 m resin-grouted rebars and chain-link wire mesh. Fiber-reinforced shotcrete, 3.81 to 5.1 cm thick, was also used at the LFM95-C2 site. During the period of the monitoring, mining was conducted in the area indicated in Figure 18.18 from a depth of 1,579 to 1,606 m below ground surface.

Figure 18.19 shows a cross section of the excavation and location of the instruments for both sites. These cross sections depict the view facing the orebody. Five 5-anchor rod extensometers were installed per site. The extensometer holes were 7.6 cm in diameter. The deep anchor was at approximately 7.9 m down hole, with anchors at roughly 1.5-m intervals. Hydraulically inflated anchors were used to ensure a nonslipping grip. The rod displacement is



(a) LFM 95-C1 Site



(b) LFM 95-C2 Site

Figure 18.19. Instrumentation array of cross sections of the 5210 level.

sensed by linear potentiometers in the extensometer head, which has a range of 5 cm. The circled numbers in Figure 18.19 denote the extensometer hole numbers for each site.

The layouts for the extensometers are essentially the same for both sites except for the extensometer hole No. 5 at the LFM95-C2 site. This hole was drilled at 15° downward relative to the horizontal axis to avoid a potential interference with an up ramp excavation nearby. Point anchors were installed for the measurement of vertical and horizontal closures at both sites. A

tape extensometer was used to take closure measurements. Also at each site, one triaxial velocity gauge was grouted into a horizontal borehole about 0.3-m deep for monitoring mining-induced seismic signals.

The extensometer readings were taken automatically via a data acquisition system at an interval of 2.25 hr. This system consisted of two primary components: two underground dataloggers and a surface personal computer. Seismic signals at the site were monitored through a mine-wide macro-seismic monitoring system developed by the U.S. Bureau of Mines, Spokane Research Center. Closure of the excavation was measured manually every 2 weeks.

18.4.2 Results of Field Monitoring

More than 50 seismic events with a magnitude greater than 1 on the Richter scale were recorded during the period of the study. The maximum magnitude experienced was about 3.5. In general, for all the seismic events that were observed, the durations of vibration were relatively short. Most events were over within 0.5 sec. It was therefore not possible to evaluate the potential impact of event durations on mechanical response. The source locations of these events were estimated through a trial-and-error process, with an approximate error of 7.62 m, using measured first-arrival times of seismic signals at different monitoring locations in the mine.

Figure 18.20 shows a set of typical results from extensometer (EXT) measurements. Position (Pos) Nos. 1 through 5 in each of the figures indicate the anchor positions for an individual extensometer with Pos No. 1 closest to and Pos No. 5 farthest from the excavation. Displacements shown in the figures were measured relative to the assembly head of the extensometer, which is at the collar of the borehole. The recorded displacements were the results of mining-related activities and mining-induced seismic events. Positive values indicate that an anchor and its corresponding assembly head moved away from each other while negative values mean that the two move toward each other.

General observation of Figure 18.20 indicates that the anchor movements were of two types. The first type showed a gradual increase in displacement. This increase is believed to be a result of mining, which induces stress redistribution, and perhaps time-dependent behavior of the rock mass (creeping). The second type of displacement exhibits a distinct pattern of step increase or decrease in displacements. This type of behavior may be attributed to slip of a joint or a fracture located between an anchor and the assembly head. This joint slip is triggered by stress changes in the region. The stress changes may be either gradual or sudden and induced by mining, mining-induced seismicity, rock mass time-dependency, and other mining-related activities.

Figure 18.21 shows the closure of the cross section of the excavation for the LFM95-C2 site. More than 220 mm of horizontal closure and 113 mm of vertical closure were observed at the site. The closure curves are broken into line segments to show the effects of seismic events. Both horizontal and vertical closures for the LFM95-C2 site gave a clear sign of seismic effects. Large closures were observed after the March 21, May 22 and 23, and November 11, 1991 events. This observation corresponds well with the extensometer measurements. The closure readings also indicate the effects of the July 31, 1991 and March 27, 1992 events (199 mm/sec, magnitude 2.0), neither of which had any impact on extensometer readings. It is interesting to note that the November 11 event (221 mm/sec, magnitude 2.5) induced more than 50 mm of horizontal

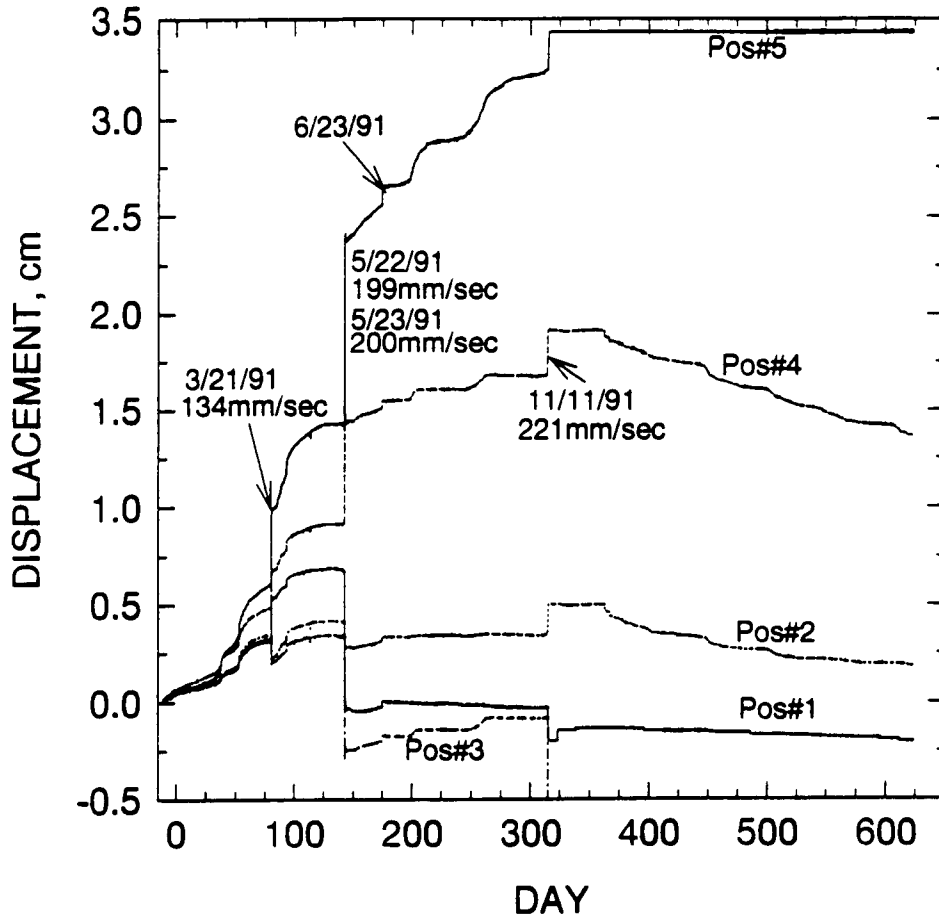


Figure 18.20. Displacement measurement for EXT No. 1 at LFM95-C2 site.

closure, which is substantially greater than the horizontal closure induced by the combined effects of the May 22 and 23 events (199 and 200 mm/sec, magnitude 2.5).

Based on the available data, it has been shown that the rock mass at the LFM95-C2 site responded to seismic events of similar or even smaller peak particle velocities with considerably higher displacements than that at the LFM95-C1 site. This phenomenon may be related to differences in the state of stresses at the two sites. As stated earlier, the LFM95-C2 site was about 30.5 m and the LFM95-C1 site was about 76.2 m away from the portion of the orebody where mining occurred during this study. Considerably higher stresses would be expected around the former site relative to the latter site as a result of the mining. The fact that greater closures occurred at the LFM95-C2 site tends to confirm the hypothesized difference in the states of stresses, assuming the rock mass and its behavior is similar at both sites. Normally, a rock mass is relatively weaker when under a higher stress condition, partly because the rock strength is known to be time-dependent. Also, it may require a relatively smaller amount of additional stresses to

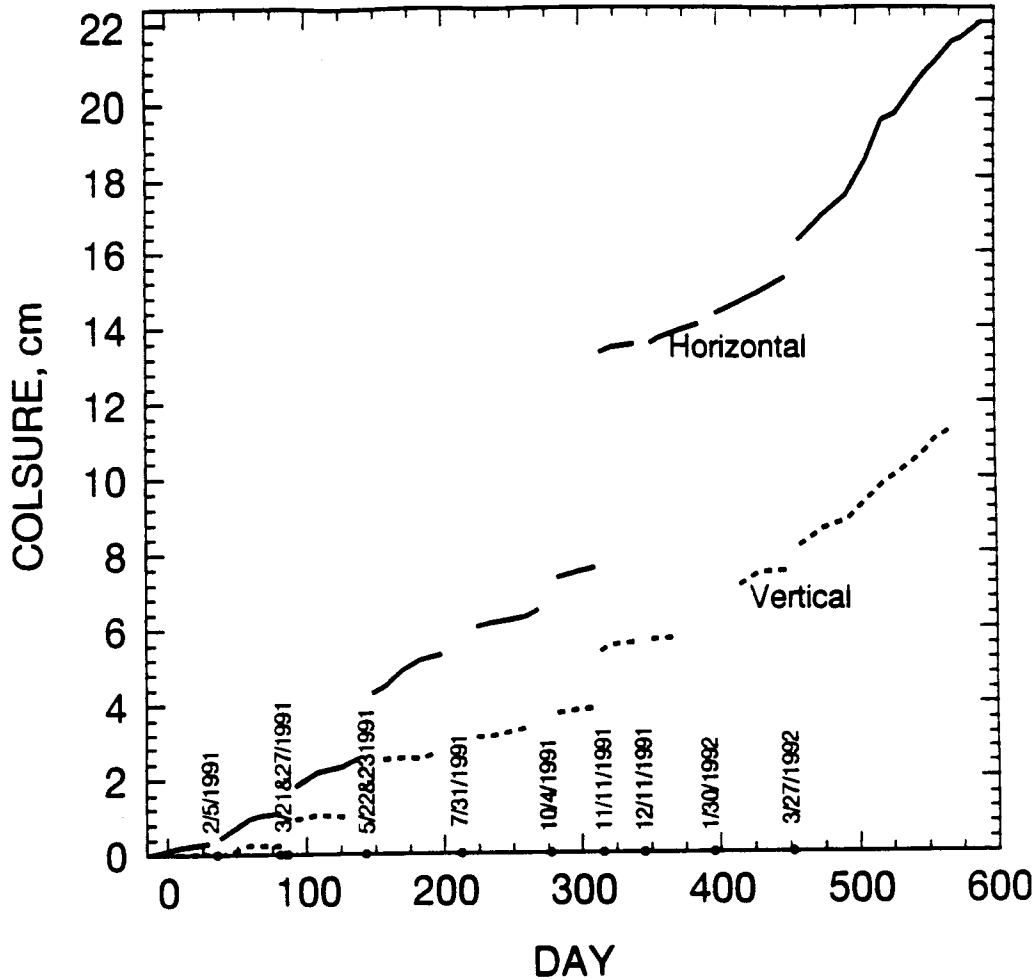


Figure 18.21. Excavation closure measurement at the LFM95-C2 site.

induce instability in a rock mass that is originally subjected to a higher state of stress. It is therefore logical to conclude, and has been demonstrated by field observation, that the LFM95-C2 site should be more vulnerable to seismic motions.

18.5 CONCLUSIONS

Experimental studies on both the dynamic behavior of single jointed rock specimens in the laboratory as well as multiple jointed rock masses in both the laboratory and field are presented. The direct shear tests on the Apache Leap welded tuff blocks containing a single, natural fracture showed that the shearing response, namely the shear resistance, could be markedly different in the forward and reverse directions depending on the joint roughness, with the shear resistance in the reverse direction being smaller. As discussed in this chapter, this is a direct consequence of the irregular roughness and interlocking nature of the mated joint surfaces. As a result, constitutive

models used in dynamic studies for underground tunnel design purposes should take into account the changes in joint shear resistance with cyclic loading of the joint. The joint dilation response during either harmonic or earthquake loading showed very little hysteresis between the forward and reverse shearing directions as compared to similar dilation measurements taken during pseudostatic direct shear tests. For the most part, the dilation that takes place during forward shearing is fully recovered during shear reversal, with perhaps a small offset due to buildup of gouge within the joint.

Both the laboratory-scale model experiment and the Lucky Friday Mine field experiment to assess the dynamic behavior of a jointed rock mass containing a tunnel showed that the primary mode of deformation of the rock mass was due to stick-slip behavior along the joints. This stick-slip behavior seems to explain quite well the phenomenon of the excavations responding to some seismic events but being unresponsive to others. If the incoming seismic wave cannot provide sufficient energy to increase the shear stress to a level that exceeds the residual shear strength, it is not likely to cause joint slip. It should be noted, that the shear strength may also be reduced with a temporary reduction in normal stress across the joint from seismic wave reflections. The degree to which the seismic motion, or other mining related activities, influences this stick-slip type joint behavior depends on how close the joint is to its residual strength envelope. The joint stick-slip behavior forms a basis for the progressive accumulation of joint permanent deformation and, consequently, rock mass fatigue. Materials are normally weaker under fatigue conditions. This weakened condition implies that similar, or even more, damage to an excavation may be realized through a number of seismic events with relatively smaller magnitudes, as opposed to the damage due to a single seismic event with a strong motion (in terms of peak particle velocity).

18.6 REFERENCES

- Brown, E.T., and J.A. Hudson. 1974. Fatigue failure characteristics of some models of jointed rock. *Earthquake Eng. and Struct. Dyn.* Vol. 2. pp. 379-386.
- Hsiung, S.M., A.H. Chowdhury, W. Blake, M.P. Ahola, and A. Ghosh. 1992a. *Field Site Investigation: Effect of Mine Seismicity on a Jointed Rock Mass*. CNWRA 92-012. San Antonio, TX: Center for Nuclear Waste Regulatory Analyses.
- Hsiung, S.M., W. Blake, A.H. Chowdhury, and T.J. Williams. 1992b. Effects of mining-induced seismic events on a deep underground mine. *PAGEOPH*. Vol. 139. No. 3/4. pp. 741-762. Basel: Birkhauser Verlag.
- Jing, L., E. Nordlund, and O. Stephansson. 1992. An experimental study on the anisotropic and stress-dependency of the strength and deformability of rock joints. *Int. J. Rock Mech. Min. Sci. & Geomech. Abstr.* Vol. 29. No. 6. pp. 535-542. New York, NY: Pergamon Press.
- Bakhtar, K., and N. Barton. 1984. Large Scale Static and Dynamic Friction Experiments. *Proceedings of the 25th U.S. Symposium on Rock Mechanics*. Dowding and Singh (eds). pp. 457-466. Baltimore Maryland: Port City Press.
- Gillette, D.R., S. Sture, H.K. Ko, M. Gould, and G. Scott. 1983. Dynamic behavior of rock joints. *Proceedings of the 24th U.S. Symposium on Rock Mechanics*. pp. 163-179.
- Hobbs, B.E., A. Ord, and C. Marone. 1990. Dynamic behavior of rock joints. *Rock Joints*. Barton & Stephansson (eds). pp. 435-445. Rotterdam, Netherlands: A.A. Balkema.

- Barla, G., M. Barbero, C. Scavia, and A. Zaninetti. 1990. Direct shear testing of single joints under dynamic loading. *Rock Joints*. Barton & Stephansson (eds). pp. 447-454. Rotterdam, Netherlands: A.A. Balkema.
- Crawford, A.M., and J.H. Curran. 1981. The influence of shear velocity on the frictional resistance of rock discontinuities. *Int. J. Rock Mech. Min. Sci. & Geomech. Abstr.* Vol. 18. pp. 505-515. New York, NY: Pergamon Press.
- Barton, N., and V. Choubey. 1977. The shear strength of rock joints in theory and practice. *Rock Mechanics*. Vol. 10. pp. 1-54.
- Hsiung, S.M., D.D. Kana, M.P. Ahola, A.H. Chowdhury, and A. Ghosh. 1994a. *Laboratory Characterization of Rock Joints*. NUREG/CR-6178. Washington, DC: U. S. Nuclear Regulatory Commission.
- Hsiung, S.M., M.P. Ahola, D.D. Kana, A.H. Chowdhury, and S. Mohanty. 1994b. *NRC High-Level Radioactive Waste Research at CNWRA January-June 1994 - Chapter 2: Rock Mechanics*. CNWRA 94-01S. San Antonio, TX: Center for Nuclear Waste Regulatory Analyses.
- Hsiung, S.M., A. Ghosh, A.H. Chowdhury, and M.P. Ahola. 1995a. Laboratory investigation of rock joint dynamic behavior. *Proceedings of the 35th U.S. Symposium on Rock Mechanics*. Rotterdam, Netherlands: A.A. Balkema. (In publication).
- Kana, D.D., D.C. Scheidt, B.H.G. Brady, A.H. Chowdhury, S.M., Hsiung, and B.W. Vanzant. 1990. *Development of a Rock Joint Dynamic Shear Test Apparatus*. CNWRA 90-005. San Antonio, TX: Center for Nuclear Waste Regulatory Analyses.
- Kana, D.D., A.H. Chowdhury, S.M. Hsiung, M.P. Ahola, B.H.G. Brady, and J. Philip. 1992. Experimental techniques for dynamic testing of natural rock joints. *Proceedings of the 7th International Congress on Rock Mechanics*. pp. 519-525.
- Board, M.P., and Beus, M.J. 1989. *In Situ measurements and preliminary design analysis for deep mine shafts in highly stressed rock*. Report of Investigations. RI 9231. Washington, DC: U.S. Bureau of Mines.
- Huang, X., B.C. Haimson, M.E. Plesha, and X. Qiu. 1993. An investigation of the mechanics of rock joints - Part I. Laboratory investigation. *Int. J. Rock Mech. Min. Sci. & Geomech. Abstr.* Vol. 30. No. 3. pp. 257-269.
- Wibowo, J.T., B. Amadei, S. Sture, and A.B. Robertson. 1992. Shear response of a rock joint under different boundary conditions: an experimental study. *Conference on Fractured and Jointed Rock Masses*. June 3-5, Lake Tahoe, CA.
- Hsiung, S.M., M.P. Ahola, D.D. Kana, A.H. Chowdhury, and S. Mohanty. 1995b. *NRC High-Level Radioactive Waste Research at CNWRA July-December 1994 - Chapter 2: Rock Mechanics*. CNWRA 94-02S. San Antonio, TX: Center for Nuclear Waste Regulatory Analyses.
- Kana, D.D., S.M. Hsiung, and A.H. Chowdhury. 1995. A scale model study of seismic response of an underground opening in jointed rock. *Proceedings of the 35th U.S. Symposium on Rock Mechanics*. Rotterdam, Netherlands: A.A. Balkema. (In publication).